

Conditional knock-down of a novel coccidian protein leads to the formation of aberrant apical organelles and abrogates mature rhoptry positioning in *Toxoplasma gondii*

Juliette Morlon-Guyot^{a,1}, Laurence Berry^{a,1}, Isabelle Sauquet^{a,1}, Gurman Singh Pall^{b,c,1}, Hiba El Hajj^{d,1}, Markus Meissner^{b,c}, Wassim Daher^{a,*}

^a *Dynamique des Interactions Membranaires Normales et Pathologiques, UMR5235 CNRS, INSERM, Université de Montpellier, Montpellier, France*

^b *Wellcome Centre for Molecular Parasitology, University of Glasgow, Glasgow, UK*

^c *Department of Veterinary Sciences, Experimental Parasitology, Ludwig-Maximilians-Universität, München, 80802, Munich, Germany*

^d *Departments of Internal Medicine and Experimental Pathology, Immunology and Microbiology, American University of Beirut, Beirut, 1107 2020, Lebanon*

ARTICLE INFO

Keywords:

Toxoplasma gondii
Rhoptry positioning
Microneme biogenesis
Invasion
CORVET and HOPS

ABSTRACT

Toxoplasma gondii which is a member of the coccidian parasites owns a spatially polarized secretory system, which synthesizes *de novo* micronemes and rhoptries. These apical secretory organelles discharge their contents into host cells promoting invasion and survival. Herein, we identified a novel Coccidian Specific CORVET/HOPS Associated Protein (CSCHAP) belonging to the interaction network of both tethering complexes. CSCHAP is associated with the endomembrane system, rhoptries, micronemes and probably to the inner core of the conoid. Conditional depletion of CSCHAP leads to apical disconnection of rhoptries, aberrant apical organelles biogenesis and severely hinders *T. gondii* invasion. Overall, our study provides new insights into the mechanisms underpinning secretory organelles biogenesis in coccidian parasites.

1. Introduction

Apicomplexan parasites are a phylum of obligate intracellular protists, responsible for a wide range of human and animal afflictions. Among these, *Plasmodium* species are the causative agent of malaria and *Toxoplasma gondii* (*T. gondii*) is responsible for toxoplasmosis.

Apicomplexans are named after an apical complex structure containing among others unique secretory organelles playing a key role in their invasion [1]. This apical complex contains rhoptries and micronemes that sequentially discharge their contents, enabling parasite gliding motility, invasion and intracellular survival [2]. In *T. gondii*, the apical complex also includes a cytoskeletal component termed the conoid, which is connected to two pre-conoidal rings (PCR) at the top and an apical polar ring (APR) at the bottom [1]. The conoid is formed by a unique polymer of 14 tubulin fibers arranged as a set of counter-clockwise spiraling filaments, creating a cone-shaped structure [3]. The conoid protrudes and its extrusion may play a role in coccidian parasites motility, invasion and egress [4]. In addition, two intra-conoid microtubules have been identified, both are positioned close to the center of the apical complex [5].

Host cell entry is initiated by the attachment and reorientation of the polarized parasites, such that the apical secretory organelles (micronemes and rhoptries) sequentially discharge their contents at the point of contact with the host plasma membrane [6]. It has been suggested that the intra-conoid microtubules are closely associated with rhoptries and micronemes and are speculated to provide structural support for both secretory organelle positioning and for their protein secretion during invasion [5]. Micronemes and rhoptries, secrete their contents at the tip of the apex. Micronemes are located at the anterior part of the parasites, and their secreted micronemal proteins (MICs) are involved in gliding motility, host cell invasion and parasites exit from infected host cells [2]. Rhoptries are situated at the apical pole of the parasite and adopt an elongated, club-shaped morphology with a narrow neck and a bulbous body whose protein contents are tightly involved in parasite invasion, parasitophorous vacuole membrane (PVM) formation, and ensure the evasion of the host cell defense mechanisms [2,7–9]. To discharge and inject their contents into host cells, the neck of the rhoptries traverses the apical complex and reaches a point of contact at the apical tip of the parasite referred to as the

Abbreviations: CSCHAP, Coccidian Specific CORVET/HOPS Associated Protein; TATI-1, Trans-activator Trap identified; ARO, Armadillo Repeats Only protein; CORVET, class C core vacuole/endosome transport; HOPS, homotypic vacuole fusion and protein sorting; CAM1, calmodulin 1

* Corresponding author.

E-mail address: wassim.daher@univ-montp2.fr (W. Daher).

¹ These authors contributed equally to this work.

<https://doi.org/10.1016/j.molbiopara.2018.06.003>

Received 20 April 2018; Received in revised form 23 June 2018; Accepted 23 June 2018

Available online 27 June 2018

0166-6851/ © 2018 Elsevier B.V. All rights reserved.

porosome [10]. During parasite penetration only one or two of the 8–12 rhoptries inject their content, including rhoptry neck proteins (RONs) and rhoptry bulb proteins (ROPs), into the host cell [6,11]. RONs initiate the formation of a moving junction (MJ) required for host cell invasion and ROPs hijack host cell functions to assist parasite survival [8,11].

Pro-micronemes and pro-rhoptries are formed *de novo*, first appearing as vesicles in close proximity to the Golgi complex, and then subsequently maturing into micronemes and rhoptries organelles [12]. Many protein complexes involved in canonical vesicular trafficking in mammals, such as retromer complex, adaptin protein complex 1, clathrin complex, CORVET and HOPS complexes are involved in the biogenesis of micronemes and rhoptries [12,13]. The armadillo repeats only protein (ARO) located at the surface of rhoptries is a key factor ensuring the apical positioning and clustering of rhoptries [14–16]. Conditional depletion of ARO and MyoF, or interfering with actin polymerization lead to the random dispersion of rhoptries within the parasite cytosol, block rhoptry secretion and impede host cell invasion [14,15,17]. Two other proteins called ARO interacting protein (AIP) and adenylate cyclase β (AC β) were found to be associated with the ARO complex but do not seem to have an apparent role in rhoptry positioning at the apical pole of *T. gondii* tachyzoites [16].

In this study, we characterized a novel coccidian-specific protein belonging to the interaction network of *Toxoplasma* Vps11 protein (a common member of CORVET and HOPS tethering complexes). In contrast to Vps11 mutant where a general block in the biogenesis of dense granules, micronemes, rhoptry and VAC compartment was obtained, the novel coccidian-specific protein shows a more restricted function, and intervenes in the apical positioning of mature rhoptries. Moreover, its depletion leads to the formation of aberrant apical organelles.

2. Materials and methods

2.1. Parasite culture

Toxoplasma gondii RH strains RH-ku80ko [18] and TATI1-ku80ko [19] were grown in HFFs maintained in Dulbecco's modified Eagle's medium (DMEM; GIBCO, Invitrogen) supplemented with 5% fetal calf serum (FCS) and 2 mM glutamine. Selections of transgenic parasites were performed with chloramphenicol for CAT selection [20], pyrimethamine for DHFR-TS selection [21], 1 μ M Shld-1 for DD fusion stabilization [22] and ATc at 1.5 μ g/ml for the inducible system [23].

2.2. *Toxoplasma* vectors and generation of transgenic *T. gondii* parasites

Plasmids LIC-CAT-CSCHAP/Ctg-GFP and LIC-CAT-CSCHAP/Ctg-HA₃ were designed to add a sequence coding for a GFP or (3) HA at the endogenous locus of TgCSCHAP open reading frame. A 1204 bp fragment corresponding to the 3' of TgCSCHAP was amplified from genomic DNA and cloned into LIC-CAT-GFP or LIC-CAT-HA₃ vectors [18]. 40 μ g of these plasmids was digested by PshAI restriction enzyme and then transfected in the RH-ku80ko or cschapi or vps11i strains and were subjected to chloramphenicol selection.

A 1398 bp fragment corresponding to the 5' of the TgCSCHAP coding region (downstream of the codon corresponding to the first predicted in-frame methionine residue) was amplified by PCR from *T. gondii* genomic DNA and then cloned in the DHFR-tetO7-Sag4 plasmid between BglII and NotI restriction sites [19,24], downstream the DHFR selection marker, tetO7 tet operator and pSag4 promoter. This construct was linearized by XmaI prior to transfection. Transfected TATI1-ku80ko parasites were selected with pyrimethamine and cloned by limit dilution. Positive clones were verified by PCR to detect the native locus or the single homologous recombination of the inducible vector in the CSCHAP locus.

To detect the outer core of the conoid, the apical polar ring and the ELC, the cschap-HA₃ strain was transfected transiently with 100 μ g of

RING1-YFP or CAM1-GFP or DD-Myc-Rab5 A or DD-Myc-Rab7 circular vectors, respectively [25–27].

2.3. Protein detection by Western blot

To detect CSCHAP-GFP, CSCHAP-HA₃, CSCHAPi-HA₃, GFP, Vps11-HA₃, ARO or MIC2, ROP5, GRA3 proteins, parasite lysates or eluted proteins were separated on 3–8% or 10% acrylamide gels depending on their size prior to detection. Upon transfer to nitrocellulose membranes, the blots were probed with appropriate antibodies in 5% non-fat milk powder in TNT buffer (50 mM Tris pH 8; 150 mM NaCl; 0.05% Tween-20) (EUROMEDEX). The primary antibodies used and their respective dilutions were rat anti-HA (Roche) at 1/300, rabbit anti-GFP (abcam) at 1/1000, mouse anti-ROP5 at 1/100, mouse anti-MIC2 at 1/100, rabbit anti-ARO at 1/1000 and mouse anti-GRA3 at 1/1000. Bound secondary conjugated antibodies were visualized using either the ECL system (Amersham Corp.) or using alkaline phosphatase kit according to manufacturer's instructions (Promega).

2.4. Fluorescent staining of cells

Briefly, for IFAs of intracellular parasites, infected confluent HFF monolayers were fixed for 20 min in 4% paraformaldehyde in phosphate buffered saline (PBS) or with cold methanol for 6 min, permeabilized with 0.2% tritonX-100, blocked with 10% FCS in PBS and then incubated with primary antibodies [anti-HA (Roche) 1:100, anti-GFP (abcam) 1:2000, anti-SAG1 1:1000 [28], anti-MIC3 1:500 [29], anti-ROP1 1:1000 [30], anti-ROP7 1:1000 (kindly provided by Dr Peter Bradley), anti-AMA1 1:1000 [31], anti-GRA2 1:1000 (kindly provided by Dr Marie-France Cesbron), anti-CPL 1:500 [32], anti-prom2 AP 1:400 (kindly provided by Dr Vern Carruthers), anti-proROP4 1:100 (kindly provided by Dr Gary Ward), anti-MIC2 1:400 [29], anti-GAP45 1:2000 [33], anti-ARO 1:1000 [15], anti-DD 1:1000 (abcam), anti-ROP2,4 (kindly provided by Dr Jean-François Dubremetz)], followed by goat anti-rabbit or goat anti-mouse or goat anti-rat immunoglobulin G conjugated to Alexa Fluor 488 or Alexa Fluor 594 (Molecular Probes, Invitrogen). Coverslips were mounted onto microscope slides using Immumount (Calbiochem). Samples were observed with a Zeiss Axioimager epifluorescence microscope equipped with an apotome and a Zeiss AxioCam MRmCCD camera driven by the Axio vision software (Zeiss) at the Montpellier RIO imaging facility.

2.5. Super resolution microscopy

For immunofluorescence analysis, HFF cells grown to monolayer on coverslips were inoculated with *T. gondii* parasites. At 2–4 PV cell stage parasite cells were fixed with 4% w/v paraformaldehyde in phosphate buffered saline (PBS) for 20 min at room temperature. Fixed cells were permeabilized and blocked with 0.2% Triton-X100, 2.5% bovine serum albumen (BSA) in PBS and stained with primary antibodies: rabbit anti-GAP45 (kind gift from Dominique Soldati), mouse anti-ROP2/4 (T3 4 A7) and rat anti-HA (ROCHE cat # 1,187,431,001). Secondary antibodies used were goat anti-rabbit Alexa Fluor 594, goat anti-mouse 633 or goat anti-rat Alexa Fluor 488 as required (Life Technologies). Super resolution microscopy (SR-SIM ELYRA S.1 Zeiss) with a Plan Apochromat 63 \times , 1.4 NA oil immersion lens was used to capture images using a CoolSNAP HQ camera (Photometrics). Image processing, Structured Illumination Microscopy (SIM) and channel alignment, was done using ZEN Black software (Zeiss) followed by 3D construction using Imaris Image Analysis Software (Bitplane).

2.6. Plaque assay

Fresh monolayers of HFF on circular coverslips were infected with parasites in the presence or absence of 1.5 μ g/ml ATc for 7 days. Fixation, staining and visualization were performed as previously described [34].

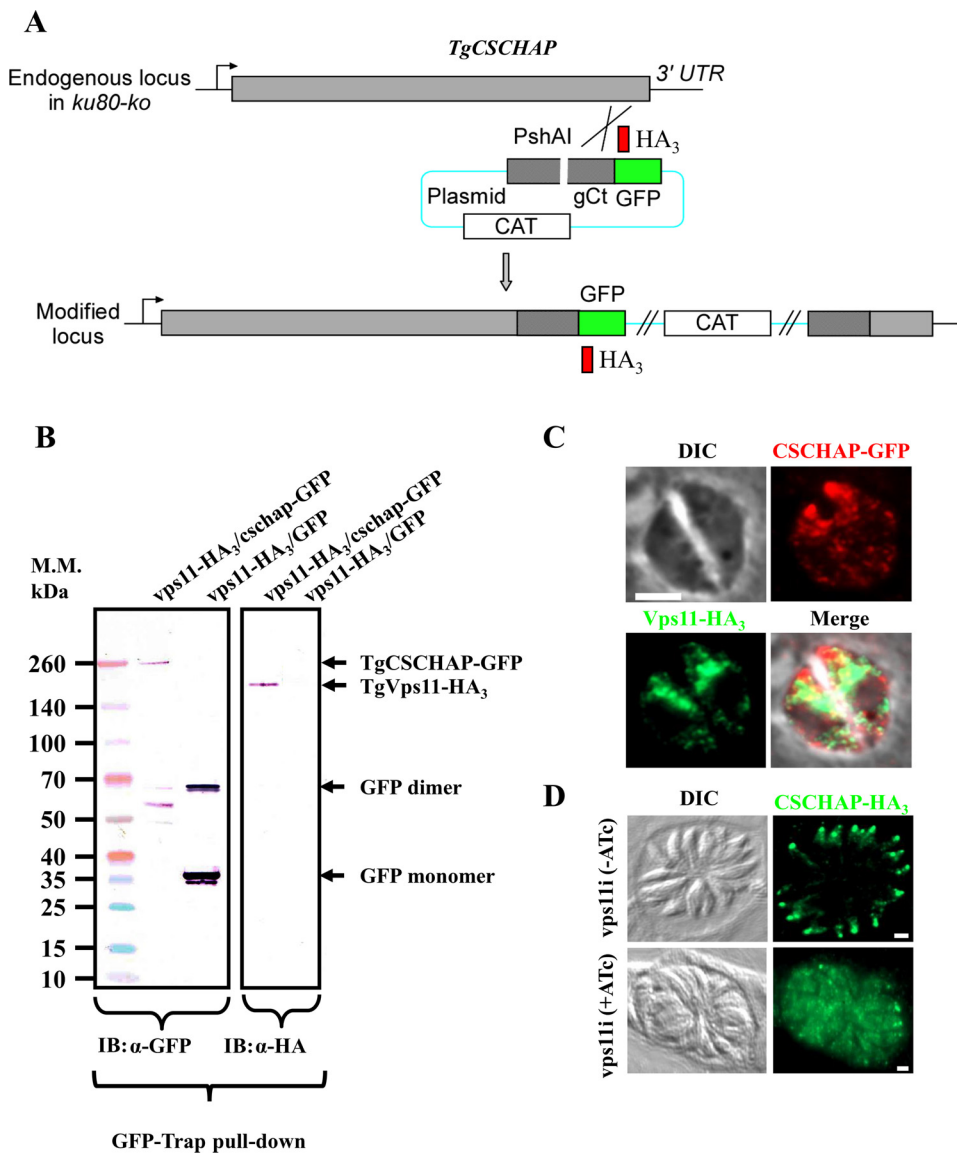


Fig. 1. TgCSCCHAP belongs to the interaction network of CORVET and HOPS tethering complexes. (A). Insertion of a GFP or three HA tags at the C-terminus of TgCSCCHAP, by single homologous recombination at the 3' of the corresponding gene (knock-in in RH-ku80ko strain). The genomic C-terminal sequence of *CSCCHAP* gene was amplified by PCR from genomic DNA using primers 5'-TAC TTCCAATCCAATTTAAtgccgacgggtctcgacactgcag-3' and 5'-tctccactccaatttagcTCTCCGTCGTGGCG TGTAGAACG-3' and cloned into both LIC-CAT-GFP and LIC-CAT-HA₃ vectors. The RH-ku80ko strain was transfected with 30 μg of the resulting plasmids and transgenic parasites selected in presence of chloramphenicol. (B). To highlight the interaction of TgCSCCHAP with TgCORVET and TgHOPS, we generated two different cell lines. In the first one, the endogenous proteins TgCSCCHAP and TgVps11 were fused to a GFP and 3-HA tags, respectively. The second one that expresses the GFP protein alone and the native TgVps11 protein fused to 3-HA tags was used as negative control. Pull-down experiments were carried out using the GFP-Trap system. Proteins that bind to GFP or to TgCSCCHAP-GFP were eluted and subjected to western blot analysis with anti-GFP (left lanes) and anti-HA (right lanes) antibodies. IB: immunoblot. (C). Co-staining between GFP- tagged TgCSCCHAP and endomembrane marker TgVps11-HA₃. DIC: differential interference contrast. (D). Immunofluorescence assays of TgCSCCHAP-HA₃ in intracellular *vps11i* parasites grown in the presence or absence of ATc for 2 days. TgCSCCHAP-HA₃ was detected using anti-HA antibodies. IFA scale bars represent 2 μm.

2.7. Intracellular growth assays

Parasites (*cschapi*) were pretreated for 48 h, with or without 1.5 μg/ml ATc, collected promptly after egress and inoculated onto new HFF monolayers in the absence or presence of ATc during 24 h. The infected host cells were then fixed with PFA and stained with anti-TgGAP45 antibodies. The numbers of parasites per vacuole in more than 300 vacuoles for each condition were counted. Data are mean values ± standard deviation (S.D.) from three independent biological experiments.

2.8. Invasion assays

Parasites were treated for 72 h with or without 1.5 μg/ml ATc, and collected promptly after egress. For invasion assays, 5 × 10⁶ freshly released tachyzoites were sedimented on confluent cells for 30 min on ice, then warmed up for invasion for 5 min at 38.5 °C. Invasion was stopped by fixation in 4% PAF and parasites were further processed for IFA. Prior to triton permeabilization, extracellular parasites were labelled with anti-SAG1 antibodies, while following permeabilization, intracellular parasites were stained with the anti-ROP1 antibody labeling the nascent PV [35]. Data are mean values ± SD from three independent biological experiments. For each condition, 300 parasites were observed.

2.9. Egress assay

Parasites incubated with or without 1.5 μg/ml ATc for 39 h were collected promptly after egress and inoculated onto new HFF monolayers, and then incubated with ATc during 33 h to allow intracellular growth. Afterwards, the ATc containing medium was changed and infected cells were incubated in DMEM containing 0.06% of DMSO or 3 μM of the Ca²⁺ ionophore A23187 (from Streptomyces chartreusensis, Calbiochem 100,105), for 5 min at 37 °C as previously described [34]. Data are mean values ± SD from three independent biological experiments. For each condition, 300 parasites were observed.

2.10. Gliding motility assay

Parasites were incubated for 72 h in media containing 1.5 μg/ml ATc, and collected promptly after egress. Freshly released tachyzoites were collected by centrifugation, resuspended in 100 μl and deposited onto poly-L-lysine coated coverslips (1 mg/ml, 2 h at room temperature) in a wet environment for 15 min at 37 °C. Parasites were fixed with PAF/GA and IFA using the anti-SAG1 antibody was performed to visualize the trails.

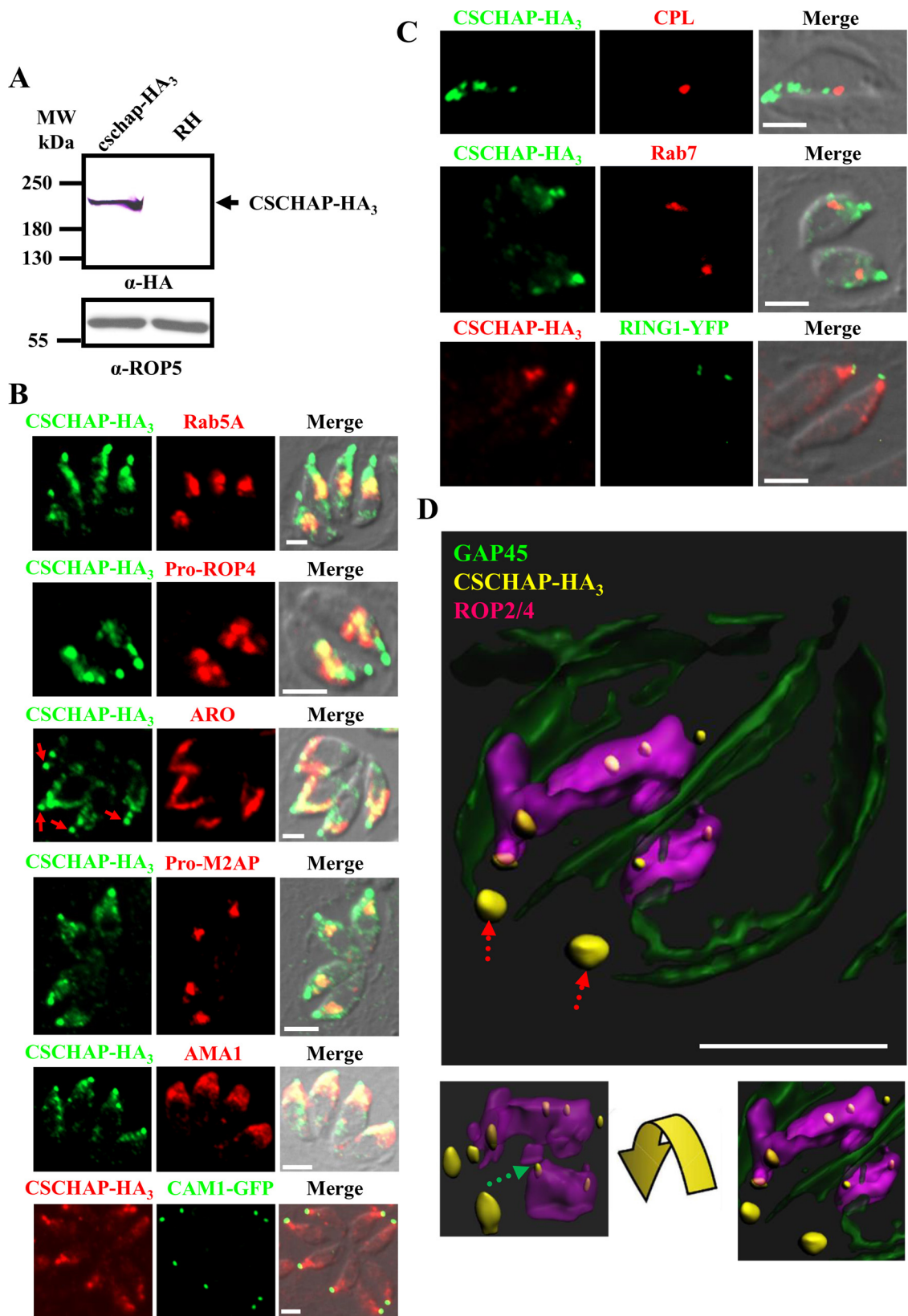


Fig. 2. Expression and localization of TgCSCHAP in tachyzoites. (A). Western blot analysis of lysates obtained from cschap-HA₃ or RH strains probed with a rat anti-HA antibody (dilution 1/1000, Roche). The ROP5 protein was used as a loading control. (B). Immunofluorescence analysis of TgCSCHAP-HA₃ parasites grown on HFF monolayers, with the indicated antibodies (pro-ROP4, ARO, pro-M2 AP and AMA1) or transiently expressing the indicated markers (DD-Myc-Rab5 A and CAM1-GFP). The extreme apical dot staining TgCSCHAP is indicated by a red arrow. (C). Immunofluorescence analysis of TgCSCHAP-HA₃ parasites grown on HFF monolayers, with the indicated antibodies (CPL) or transiently expressing the indicated markers (DD-Myc-Rab7 and RING1-YFP). IFA scale bars represent 2 μm. (D). Immunofluorescence analysis using super resolution microscopy followed by 3D reconstruction using IMARIS software of intracellular TgCSCHAP-HA₃ parasites (2 cell PV) hybridised with antibodies to detect GAP45 (pellicle marker, green), ROP2/4 (rhoptries marker, violet) and HA (CSCHAP-HA₃, yellow). Partial co-localisation of CSCHAP-HA₃ is observed with the rhoptries marker ROP2/4. Inset images show apical end of parasite, rotation of the image and removal of the IMC/GAP45 signal reveals the CSCHAP-HA₃ signal is adjacent and embedded along the length of the rhoptries. Red arrow indicates most apical CSCHAP-HA₃ staining which is probably located at the extreme apical end of parasites at the conoid area. IFA scale bar represents 2 μm.

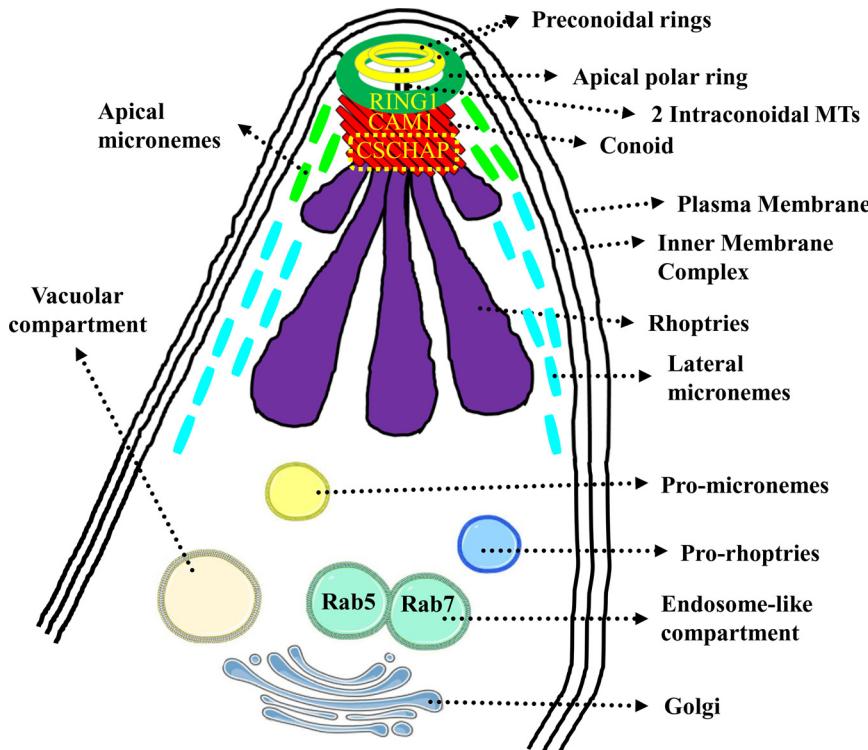


Fig. 3. Determination of the localization of TgCSCHAP protein. Schematic representation of the endomembrane system (Golgi, Endosome-like compartment, Vacuolar compartment, Pro-rhoptries and Pro-micronemes), apical secretory organelles (Rhoptries, Lateral and Apical microneemes) and apical complex (Preconoidal rings, Apical polar ring, Conoid and 2 Intraconoidal microtubules) in *Toxoplasma*. RING1 and CAM1 are markers of APR and outer conoid respectively. The yellow hatched rectangle represents the probable location of the extreme apical staining dot of TgCSCHAP.

2.11. Microneme secretion assay

Freshly egressed parasites were re-suspended in equal volume of intracellular (IC) buffer (5 mM NaCl, 142 mM KCl, 1 mM MgCl₂, 2 mM EGTA, 5.6 mM glucose, 25 mM HEPES, pH 7.2) prior to pelleting (1050 rpm/10 min). Pellets were subsequently washed in IC buffer and re-pelleted before resuspension in serum-free medium and 500 mM propranolol (37 °C/30 min). Parasites were pelleted (1000 × g/5 min/4 °C), and supernatant was transferred to new Eppendorf tubes and re-pelleted (2000 × g/5 min/4 °C). Final supernatant (excreted secreted antigens [ESAs]) was re-suspended in sample buffer (50 mM Tris-HCl [pH 6.8], 10% glycerol, 2 mM EDTA, 2% SDS, 0.05% bromophenol blue, 100 mM DTT) and boiled prior to analysis by immunoblotting using anti-MIC2 and anti-GRA3 antibodies.

2.12. Studying the interaction between CSCHAP-GFP and Vps11-HA₃

Freshly released tachyzoites were harvested, washed in PBS, and lysed in RIPA buffer (50 mM Tris HCl pH 7.4, 1% NP40, 76 mM NaCl, 2 mM EGTA, 10% Glycerol, protease inhibitor cocktail [Roche]) and incubated on ice for 20 min. After centrifugation at 14,000 rpm during 45 min at 4 °C, the supernatants were subjected to immuno-precipitation using anti-GFP lama antibodies (GFP-Trap Agarose Beads from ChromoTek). Following stringent washing conditions (50 mM Tris HCl pH 7.4, 1% Nonidet P-40, 76 mM NaCl, 2 mM EGTA, 10% Glycerol, protease inhibitor cocktail [Roche]), beads were suspended in loading buffer for SDS-PAGE, followed by western blot analysis.

2.13. Electron microscopy

Infected HFF monolayers on coverslips were fixed for 4 h at room temperature with 2.5% glutaraldehyde (EMS) in 0.1 M phosphate buffer pH7.2, washed and fixed for an additional hour in 1% Osmium tetroxide. After washing in water, infected cells were stained overnight in 2% uranylacetate. Coverslips were then dehydrated in ethanol series and embedded in Epon (Embed 812, EMS). Ultrathin sections were prepared with a Leica ultracut E microtome, contrasted with 2% uranylacetate in ethanol and lead citrate. Sections were then observed with a JEOL 1200E electron microscope.

2.14. Semi-quantitative RT-PCR

Total RNA was extracted from *T. gondii* tachyzoites using the Nucleospin RNA II kit (Macherey-Nagel, 740,955.10). RT-PCR was performed with the Superscript III first-strand synthesis kit (Invitrogen, 18080-051). Three hundred nanograms of total RNA as a template were used per RT-PCR reaction, and specific primers of TgCSCHAP or TgFYVE1 were used. Thirty cycles of PCR were performed.

2.15. Sequence alignment

Sequence of CSCHAP from *T. gondii* (TGME49_313340) was aligned to *H. sapiens* (AAF29901.1) syntaphilin and to *H. sapiens* (CAA67333.1) dynactin using the online tool Clustal Omega. The resulting sequence parts were then used to calculate the reported sequence identities.

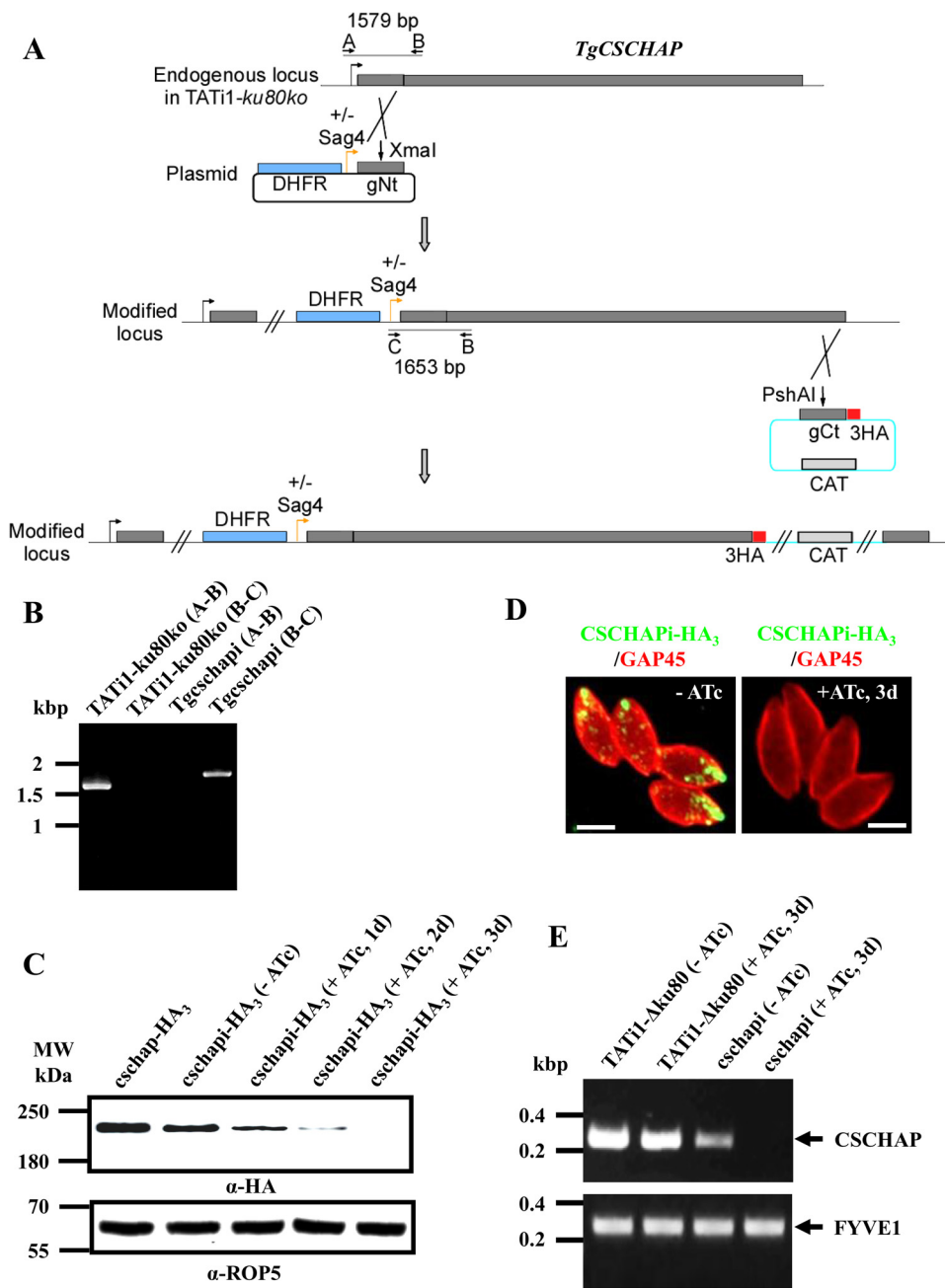


Fig. 4. Conditional disruption of *TgCSCHAP* gene and regulation of *TgCSCHAPI-HA₃* expressing parasites. (A). Schematic representation of the strategy used to replace the endogenous promoter of *TgCSCHAP* with the tetracycline-inducible promoter. The DHFR-tetO7-Sag4-NtgCSCHAP plasmid contains the dihydrofolate reductase (*DHFR*) gene (in blue) and the N-terminal genomic coding sequence of *TgCSCHAP* (in grey) under the control of the inducible tetO7Sag4 promoter (orange arrow). A 1398 bp fragment corresponding to the 5' of the coding region (downstream of the codon corresponding to the first predicted in-frame methionine residue) was amplified by PCR from *T. gondii* genomic DNA using primers 5'- ggcAGATCTATGAGCTCTCGTACCTGCGTCGTCAAC-3' and 5'- gcgcGCGGC CGCgtagtcttaagcagtcagtgccagggcagcg-3' and then sub-cloned in the DHFR-tetO7-Sag4 plasmid between BglII and NotI restriction sites downstream the DHFR selection marker, tetO7 tet operator and *pSag4* promoter. Transgenic inducible *cschapi* parasites obtained by transfecting TATI1-ku80ko strain with 40 µg of linear DHFR-tetO7-Sag4-NtgCSCHAP (digested with XmaI) and mutant parasites (*cschapi* parasites) were selected with pyrimethamine. To study the regulation of *TgCSCHAPI* gene product we inserted, by single homologous recombination, a sequence coding three HA epitope tags at the C-terminus of the corresponding *TgCSCHAPI* protein. (B). PCR analysis performed on *Tgcschapi*, showing that single homologous recombination occurred. Genomic DNA from TATI1-ku80ko parasites used as negative control. Black arrows represent the primers used for PCR analysis (A: ctgtgccttgcgtttggtctccacac; B: ccctgcttggactcttcatggaagaatcctac; C: GGGATCATTGAAAAACATCGTGAGGCTGG) and the length of the PCR fragments is indicated. (C). Western blot analysis of *TgCSCHAP-HA₃* and *TgCSCHAPI-HA₃* (± ATc) strains. *TgCSCHAPI-HA₃* parasites treated for 1, 2 and 3 days with ATc. ROP5 used as a loading control. (D). *TgCSCHAPI-HA₃* were grown for 3 days with ± ATc and assessed by IFA. Staining with anti-HA antibodies confirms *TgCSCHAPI-HA₃* knock-down in presence of ATc. Anti-GAP45 antibodies used to visualize the parasite pellicle. (E). Semi-quantitative RT-PCR analysis of *TgCSCHAP* expression in the wild-type and mutant parasites, preceded or not by 3 days of ATc treatment to regulate expression. The *FYVE1* gene was used as a loading

control. The primers that we used to amplify either a small fragment of *CSCHAP* or *FYVE1* open reading frames are as follows: CGAGAGTCGCCACCATTTGTCCG (*CSCHAP*, forward), CTCTGGGAAGACAGAGTCTGTG (*CSCHAP*, reverse), GGATCCATGAGCGAGAACGAAAATCC (*FYVE1*, forward), AAGCTTAGGTGTGAGAGGACGCACG (*FYVE1*, reverse).

2.16. Statistics

P values were calculated in the Excel software, using the Student's *t*-test assuming equal variance, unpaired samples, and using two tailed distribution. Means and SD were also calculated in the Excel software.

3. Results and discussion

To identify the interaction network of the TgVps11 protein (a central protein common to the TgCORVET and TgHOPS tethering complexes), we used the GFP-Trap pull-down strategy and we were able to identify a novel protein specific to coccidian parasites [13,36]. Since this protein is hypothetical, we named it Coccidian Specific CORVET/HOPS Associated

Protein (*CSCHAP*, TGME49_313340). To validate our mass spectrometry approach, we carried out a reverse GFP-Trap pull-down experiment. GFP and HA₃ tags were fused to the C-termini of *TgCSCHAP* and *TgVps11* respectively using the pLIC strategy (Fig. 1A). As a control, we included a strain that expresses both the native TgVps11 protein fused to HA₃ but also as well an intact GFP protein. *TgCSCHAP-GFP* and GFP proteins were pulled down using a GFP-Trap pull-down strategy. Subsequent western blot analysis using anti-GFP or anti-HA antibodies revealed the presence of *TgCSCHAP-GFP* and monomeric and dimeric GFP in the eluted fractions (Fig. 1B, left panel). Importantly, a single band at the appropriate size of *TgVps11-HA₃* was only pulled down with *TgCSCHAP-GFP* but not with GFP alone (Fig. 1B, right panel). These results confirm that *TgCSCHAP* belongs to the interaction network of TgVps11.

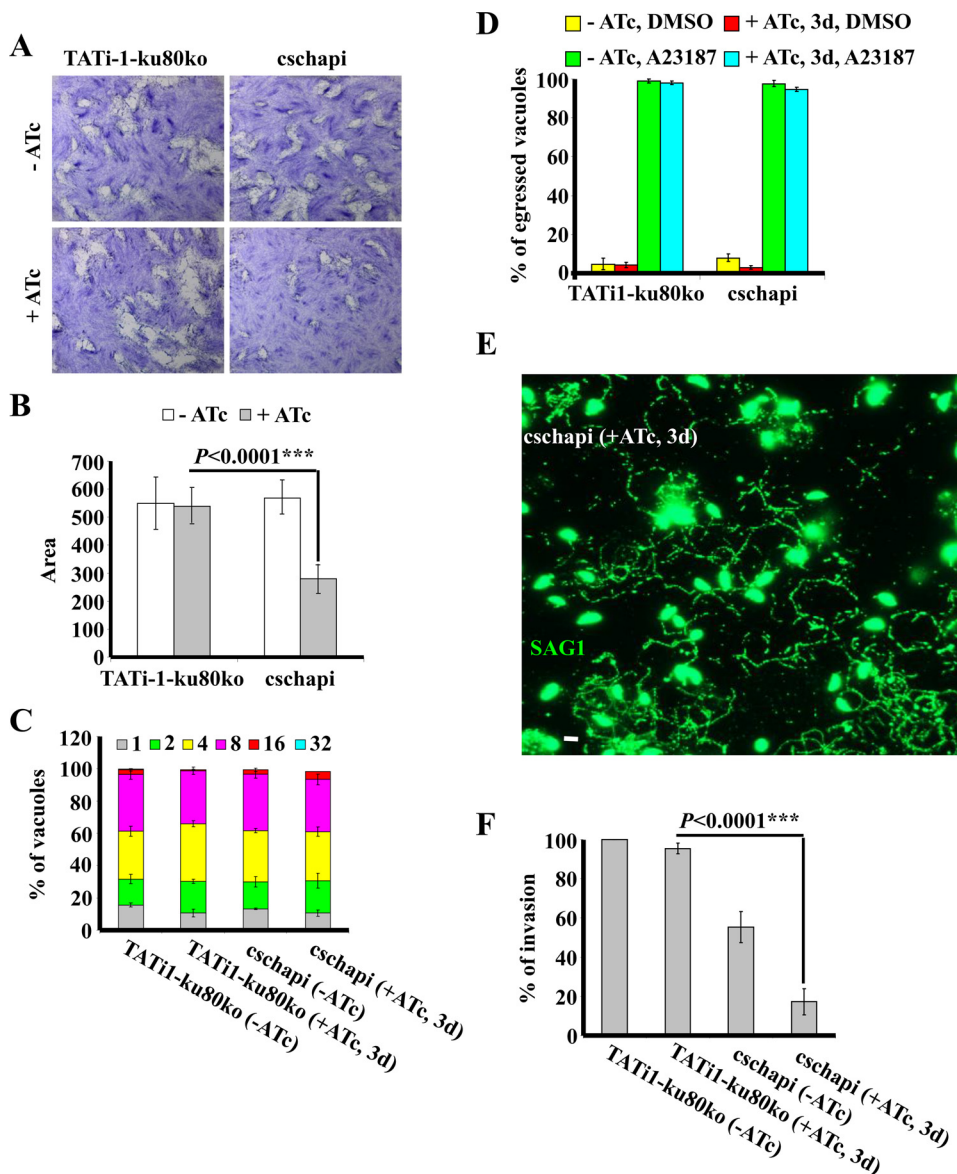


Fig. 5. Phenotypic characterization of TgCSCHAP-depleted parasites. (A). Plaque assay performed on HFF monolayer infected with TATi1-ku80ko and Tgcschapi parasites. 50 *Toxoplasma* tachyzoites from each strain \pm ATc were inoculated into 24-well plates containing confluent monolayers of HFF host cells. After 7 days \pm ATc, the HFF were stained with Giemsa. (B). The area of 30 plaques formed by each strain \pm ATc was measured by using ImageJ software (the unit of measurement that we used is Pixels). Values are means \pm standard deviations. Statistical significance was evaluated using the unpaired *t*-test $***P < 0.0001$. (C). Intracellular growth of TATi1-ku80ko and Tgcschapi cultivated in presence or absence of ATc for 2 days and allowed to invade new HFF cells. Numbers of parasites per vacuole (x-axis) were counted 24 h after inoculation, the percentages of vacuoles containing varying numbers of parasites (1, 2, 4, 8, 16, or 32 y-axis) were shown. Values are means \pm SD for three independent experiments. (D). Egress assay was performed by growing parasites for 3 days \pm ATc. Egress was induced upon addition of 3 μ M A23187, and DMSO was used as a negative control. The data shown represent mean values \pm SD from three independent experiments. (E). Gliding motility was assessed after growing Tgcschapi mutant parasites for a total of 3 days + ATc. Parasites added to Poly-L-Lysine pretreated coverslips, and trails visualized using anti-SAG1 antibodies. IFA scale bars represent 2 μ m. (F). The invasion capacity of Tgcschapi and parental (TATi1-ku80ko) parasites was evaluated after 3 days \pm ATc. Results are shown as percentage of invading parasites and values are means \pm SD for three independent experiments. Statistical significance was evaluated using the unpaired *t*-test $***P < 0.0001$.

The crosstalk between TgCSCHAP, TgCORVET and TgHOPS tethering complexes, prompted us to localize it within the parasite. Anti-GFP antibodies showed the accumulation of TgCSCHAP-GFP in vesicular structures present mainly at the apical part of the parasites but also, randomly in the cytosol (Fig. 1C). Co-localization experiments between the endomembrane protein TgVps11 and the novel TgCSCHAP-GFP protein showed a partial overlap between both proteins (Fig. 1C). Interestingly, the depletion of the TgVps11 protein disturbs the localization of endogenous TgCSCHAP-HA₃ protein, the distinct apical localization is mainly lost and a general distribution of the protein through the cytosol of the parasites is observed (Fig. 1D). These results indicate that CORVET and/or HOPS tethering complexes are responsible for the appropriate targeting of the TgCSCHAP protein. To avoid compatibility problems between antibodies and to be able to determine more precisely the localization of TgCSCHAP, we fused it with 3-HA tags (Fig. 1A). Using anti-rat HA antibodies, immunoblot analysis showed a single band corresponding to TgCSCHAP-HA₃ protein (Fig. 2A). Immunofluorescence assay (IFA) revealed that this protein localizes mainly to the apical part of the parasites (Fig. 2B and C). Co-staining with different markers revealed that TgCSCHAP colocalized partially with TgRab5 A (a marker of the endosome-like compartment), TgPro-ROP4 (a marker of immature rhoptries), TgARO (decorating the

surface of mature rhoptries), TgM2AP (a marker of immature micronemes) and TgAMA1 (a marker of mature micronemes) (Figs. 2B and 3). The larger apical dot signal labelled with TgCSCHAP was found to be systematically posterior to TgCAM1 and TgRNG1, which are proteins localizing near the middle part of the conoid, or at the APR, respectively (Figs. 2B, C and 3). Moreover, we found no obvious overlapping between TgCSCHAP and TgCPL (present in the lumen of the vacuolar compartment) or TgRab7 staining's (Figs. 2C and 3). Super resolution microscopy reveals that the CSCHAP-HA₃ signal is adjacent and embedded along the length of the rhoptries and indicates that the most apical CSCHAP-HA₃ staining is probably located at the extreme apical end of the parasites at the conoid area (Fig. 2D). These findings indicate that TgCSCHAP is associated with the Rab5 compartment, immature and mature rhoptries and micronemes and possibly with the inner part of the conoid.

To investigate the role of TgCSCHAP, we generated a conditional knock-down for TgCSCHAP (Tgcschapi), by replacing the endogenous promoter with an Anhydro-tetracycline (ATc)-repressible promoter as previously described (Fig. 4A) [24]. Single homologous integration of the inducible cassette at the TgCSCHAP locus was monitored by PCR (Fig. 4B). To study the regulation of TgCSCHAPi protein in the presence or absence of ATc, a C-terminal triple HA epitope-tag was inserted by

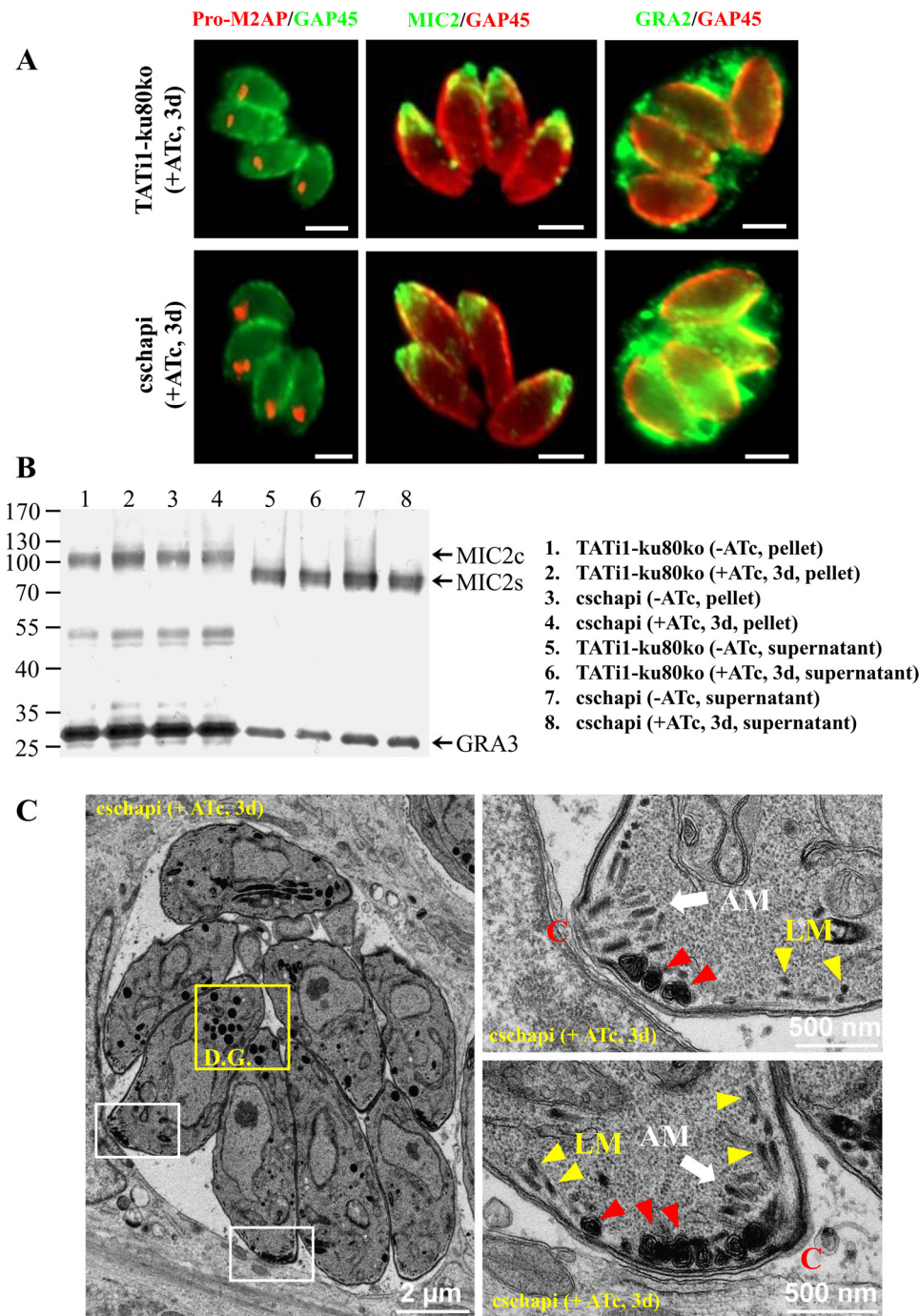


Fig. 6. Depletion of TgCSCHAP induces aberrant apical organelles but did not disturb neither the localization of immature micronemes (Pro-M2AP), micronemes (MIC2) and dense granules (GRA2) markers nor micronemes secretion. (A). TgCSCHAP-deficient parasites were incubated with ATc for 3 days. Anti-pro-M2AP, anti-MIC2 and anti-GRA2 were used to detect pro-micronemes, micronemes, and one of the secreted dense granule proteins respectively. Scale bar = 2 μm. (B). Microneme secretion assay performed on WT (TATI1-ku80ko) and Tgcschapi lines ± ATc for 3 days. Tgcschapi mutant parasites are still able to secrete their micronemes as indicated by the presence of signal when ESA (excreted secretory antigens/micronemes) was probed for MIC2 micronemal protein. Full length MIC2c protein is detected at ~100 kDa and secreted MIC2s is detected at around ~85 kDa. Microneme secretion triggered by adding propranolol (500 μM). Dense granule protein 3 (GRA3) was used as control for constitutive secretion. MIC2c: cellular and MIC2s: secreted. (C). Thin section electron micrographs taken from Tgcschapi mutant parasites grown for a total of 3 days in presence of ATc. The white inset pictures show normal apical and lateral micronemes (AM, white arrows and LM yellow head-arrows, respectively) together with aberrant compartments (red head-arrows). C: conoid, D.G.: dense granules. The morphology of dense granules seems to be intact in absence of TgCSCHAP-depleted parasites. Scale bars represent 2 μm or 500 nm.

single homologous recombination at the inducible TgCSCHAP locus in the Tgcschapi strain (Fig. 4A). A chloramphenicol acetyltransferase resistance cassette was used to select transgenic parasites expressing the inducible TgCSCHAPI-HA₃ protein (Fig. 4A). Total protein extracts of the TgCSCHAP-HA₃ and TgCSCHAPI-HA₃ (± ATc) transgenic parasites were analyzed by western blot using an anti-HA antibody; ROP5 was used as loading control (Fig. 4C). Placing the TgCSCHAP gene under the control of the minimal Sag4 promoter causes a down-regulation of the TgCSCHAPI-HA₃ protein when compared with endogenous TgCSCHAP-HA₃ levels (Fig. 4C, lane 1 vs 2). The expression of TgCSCHAPI-HA₃ is no longer detectable after 72 h of ATc treatment (Fig. 4C and D). Similarly, TgCSCHAP mRNA is drastically down-regulated under the control of Sag4 promoter without or after 3 days of ATc treatment (Fig. 4E). Depletion of TgCSCHAP results in a defect on parasite growth

as observed by plaque assays with ATc treatment (Fig. 5A). The plaques formed were reduced in size (~ 2-fold smaller), as compared to the TATI1-ku80ko wild-type strain (Fig. 5B). In addition, we observed a decrease in the number of lysis plaques formed when the TgCSCHAP protein was depleted in comparison with the control. The number of plaques formed dropped by approximately half (from 41 ± 3 to 19 ± 4 lysis plaques). The phenotypic consequences of TgCSCHAP depletion were investigated in each step of the lytic cycle. Parasite replication within host cells was scored by counting the number of parasites per vacuole after 72 h ± ATc treatment. Both examined strains replicated at a similar rate, which suggested that TgCSCHAP is not required for parasite replication (Fig. 5C). We then tested whether TgCSCHAP-depleted parasites were affected in their ability to egress from infected cells, by addition of the calcium ionophore A23187. Both

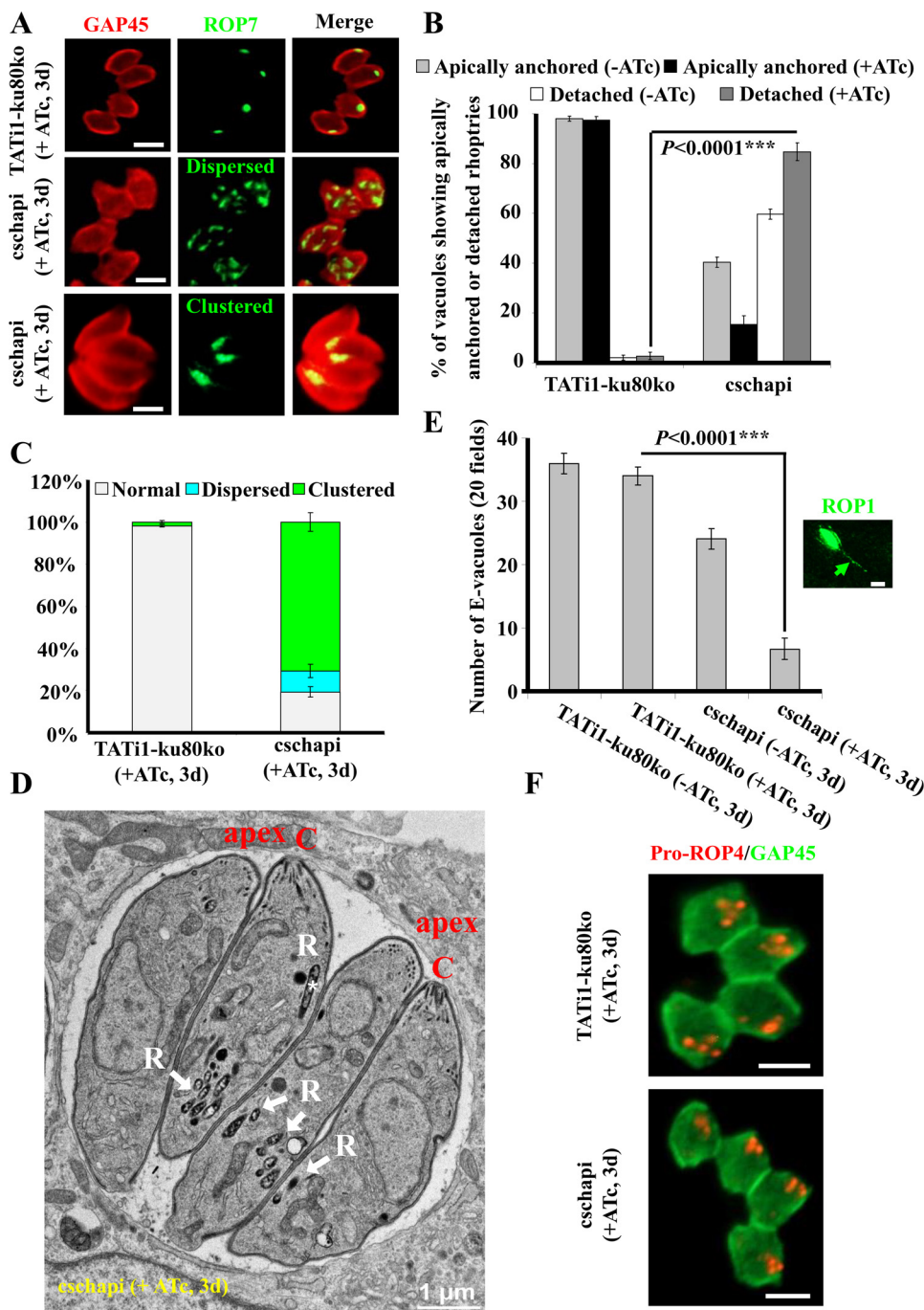


Fig. 7. Depletion of TgCSCHAP abolishes solely mature rhoptry organelle positioning to the apical end of the parasite. (A). Wild type (TATi1-ku80ko) and Tgcschapi strains were grown for 3 days + ATc and assayed by IFA using anti-ROP7 Abs. In TgCSCHAP-depleted parasites, ROP7 protein becomes spread through the whole parasite or clustered at the posterior part of parasites. (B). The localization of the rhoptries (apically anchored or detached (dispersed and clustered)) in wild type (TATi1-ku80ko) and Tgcschapi strains grown for 3 days ± ATc is reported for 100 vacuoles in three biological replicates from three independent experiments. The data shown are mean values ± SD. Statistical significance was evaluated using the unpaired *t*-test ****P* < 0.0001. (C). The localization of the rhoptries (normal, dispersed or in clusters) is reported for 100 vacuoles in three biological replicates from three independent experiments. The data shown are mean values ± SD. (D). Thin section electron micrographs taken from Tgcschapi mutant parasites grown for a total of 3 days in presence of ATc. The picture shows clustered (white arrows) and dispersed (white asterisk) mature rhoptry organelles found within the cytosol. C: conoid. Scale bar represents 1 μm. (E). Scoring the number of E-vacuoles in the parental (TATi1-ku80ko) and inducible knock-down TgCSCHAP cell lines treated ± ATc. The number of E-vacuoles in 20 fields counted following IFA using anti-ROP1 antibodies. Data are mean values ± SD for three independent experiments. Statistical significance was evaluated using the unpaired *t*-test ****P* < 0.0001. IFA scale bars represent 2 μm. (F). TgCSCHAP-deficient parasites were incubated with ATc for 3 days. Anti-pro-ROP4 antibodies were used to detect pro-rhoptries. Scale bar = 2 μm.

strains showed no defect in egress, and the percentage of lysed vacuoles was almost 100% (Fig. 5D), clearly indicating that TgCSCHAP is not required for egress. Next, we assessed whether TgCSCHAP-depleted parasites were impaired in gliding motility. TgCSCHAP-depleted strain was grown for 72 h in presence of ATc and added to poly-L-Lysine-treated coverslips. The visualization of the trails by staining for TgSAG1 deposited in the tails of gliding parasites indicates that TgCSCHAP protein is not required for parasite gliding motility (Fig. 5E). In contrast, invasion assays revealed that parasites depleted for TgCSCHAP for 72 h with ATc were significantly impaired in their ability to penetrate host cells. The percentage of invasion was reduced to ~20% compared to the control strain (Fig. 5F). In the absence of ATc, a decrease in the invasion rate of the order of 40% was observed, probably due to a lower level of expression of TgCSCHAP under the control of the inducible promoter (Figs. 4C, E and 5F). Taken together, these results show that

TgCSCHAP depletion severely and selectively affects *T. gondii* host cell invasion. To understand why TgCSCHAP-depleted parasites are affected in their ability to invade the host cell, we examined the trafficking of rhoptry, microneme and dense granule proteins by IFA and also the integrity and the positioning of the rhoptry and microneme organelles as well as dense granules by EM upon TgCSCHAP depletion. We found that TgCSCHAP depletion had no effect on the targeting or secretion of pro-micronemes, micronemes and dense granules (Fig. 6A and B). By EM, organelle morphology appeared normal, but abnormal structures were consistently observed in the apical submembrane regions flanking the conoid (Fig. 6C, red head-arrows). These structures appeared as vesicles containing an accumulation of multi-membrane whorls and were strictly apical, in a position where lateral micronemes are normally expected (Figs. 6C and S1A, yellow head-arrows). However, normal micronemes were also observed in the same mutant parasites

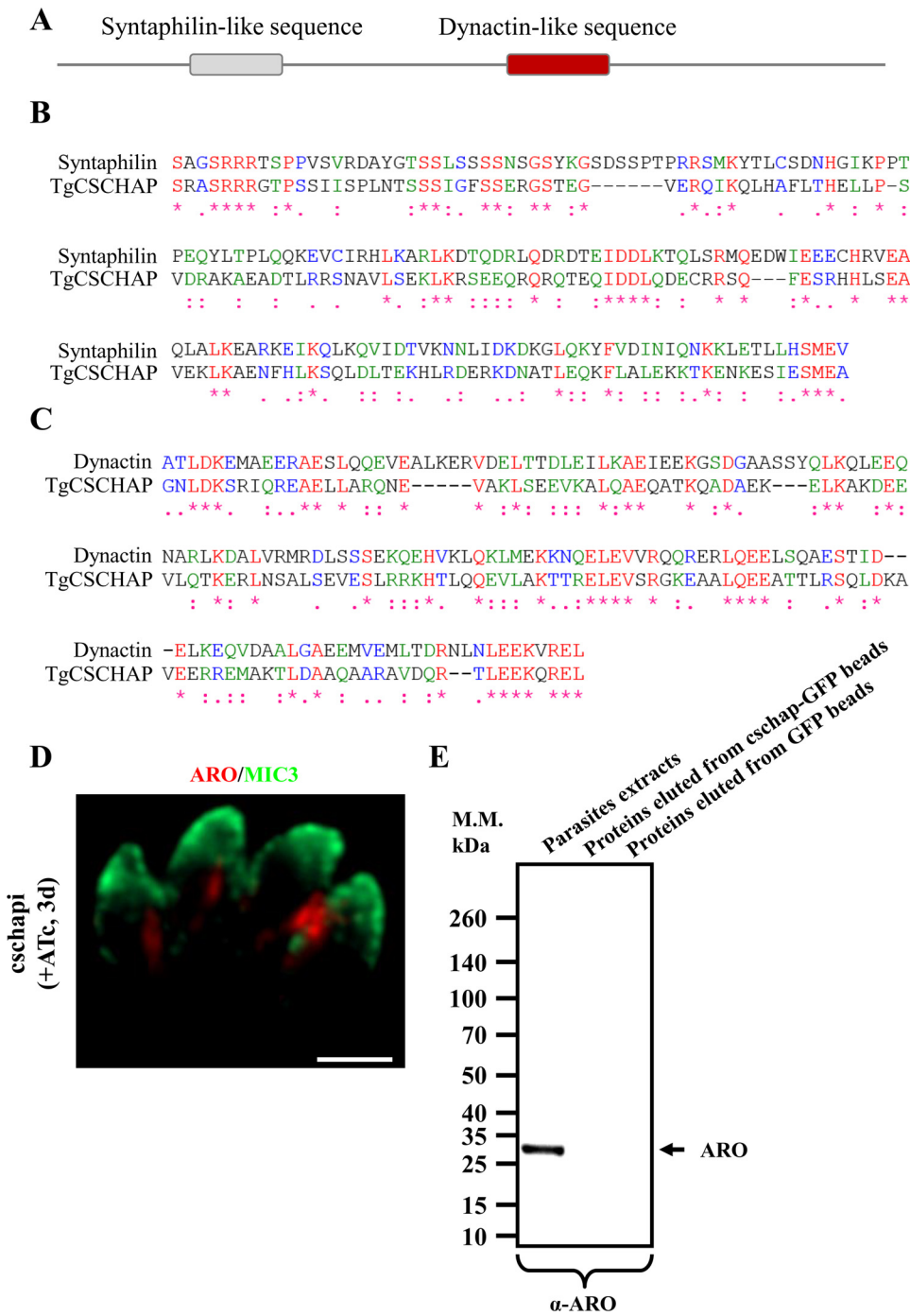


Fig. 8. (A, B and C) Primary structure of TgCSCHAP protein. (A). Schematic representation of *T. gondii* CSCHAP showing the domains of homology to syntaphilin and dynactin. (B and C). Amino-acids alignment between the putative Syntaphilin- and Dynactin-like sequences found in TgCSCHAP protein and their human homologues. (.) represents conserved residues; (:) represents similar residues; (*) represents identical residues. (D and E) The absence of TgCSCHAP does not affect the association of TgARO with rhoptries and TgCSCHAP does not seem to belong to the interaction network of TgARO. (D). Tgcschapi strain was grown for 3 days + ATc and assayed by IFA using anti-ARO and anti-MIC3 Abs. In TgCSCHAP-depleted parasites, ARO protein remains associated with rhoptries that are found on the posterior side of parasites. Scale bar = 2 μ m. (E). Western blot performed on total proteins extracts (lane 1), proteins eluted from CSCHAP-GFP beads (lane 2) and proteins eluted from GFP beads (lane 3) using anti-ARO antibodies.

(Fig. 6C, yellow head-arrows). These aberrant vesicular structures are probably much rarer in parasites not treated with ATc and therefore more difficult to observe by electron microscopy. When we examined the rhoptries, we found that when TgCSCHAP was expressed, ROP7 was associated to clustered rhoptries located at the apex of parasites (Fig. 7A–C). Interestingly, when TgCSCHAP is partially (without ATc) or fully depleted (with ATc), ROP7 was associated either to dispersed rhoptries found within the parasite cytosol (up to 10%) or to clustered rhoptries visualized on the posterior side of cschapi mutant parasites (up to 70%) (Fig. 7A–C). In contrast, using anti-Pro-ROP4 antibodies, partial or total TgCSCHAP depletion did not affect the formation of immature rhoptries (Fig. 7F). These data led us to conclude that the dispersed compartments are in fact mature rhoptry organelles that have lost their proper apical distribution and thus are unable to secrete their

content upon host cell invasion. To further validate our hypothesis, we checked by EM the positioning of rhoptries normally found in the apical part of the wild-type parasites (Fig. S1B). In TgCSCHAP-depleted parasites, we identified single organelle dispersed in the parasite cytosol (Fig. 7D, white asterisk) or a group of clustered rhoptries located at the posterior end (Fig. 7D, white arrows). The apical detachment of the rhoptries probably blocks the secretion of the rhoptry content including the RONS proteins required for the invasion process. To support this view, we counted the number of empty vacuoles (E-vacuoles, clusters of vesicles containing rhoptry proteins deposited within the host cell cytosol) in both strains \pm ATc which were detected using anti-ROP1 antibodies. Our results show a significant decrease in the number of E-vacuoles thus indicating a defect in rhoptry content secretion in the Tgcschapi mutant parasites \pm ATc (Fig. 7E). Taken

together, our data indicate that TgCSCHAP is not involved in an early step of rhoptry biogenesis but is vital for the attachment of the mature organelles to the apical end of the parasites. The potential association of TgCSCHAP with the inner part of the conoid may suggest that this protein plays a key role in anchoring rhoptries to microtubules and lies at this conoid area (Fig. 3). To gain more insight into the role of TgCSCHAP protein, we searched for putative functional domains. We identified two regions with sequence similarities with syntaphilin (amino acids 241 to 405, 26% identity and 44% similarity) and dynactin (amino acids 828 to 971, 31% identity and 48% similarity) (Fig. 8A–C). Interestingly, both dynactin and syntaphilin link vesicles or organelles to cytoskeleton by interacting with microtubules [37,38]. The presence of two putative microtubule-binding domains in TgCSCHAP suggests that the positioning of rhoptries in coccidian parasites, depends not only on actin but may also on tubulin. Future functional complementation experiments with truncated forms of the protein are needed to elucidate the role of each predicted domain in TgCSCHAP function. These experiments can be performed using the cosmid 1061064360360 and 1061064346283 that span the entire *TgCSCHAP* gene as listed on ToxoDB.

Finally, we tried to find out if there is a probable cross-talk between TgCSCHAP and TgARO. For this, we studied the localization of TgARO in the absence of TgCSCHAP and we checked for the presence of TgARO in the eluted proteins from TgCSCHAP-GFP beads. Our results show that TgARO labeling is not affected in the absence of TgCSCHAP and that TgARO does not interact directly or indirectly with TgCSCHAP (Fig. 8D and E). TgARO is associated with rhoptries detached from the apex that are visualized on the posterior side of the parasite below the micronemes. Therefore, TgCSCHAP seems to belong to a new molecular complex involved in the positioning of rhoptries in coccidian parasites. Nevertheless, we cannot rule out that such an interaction between TgCSCHAP and TgARO may be indirect and lost upon parasite lysis.

In conclusion, we identified a novel Coccidian Specific CORVET/HOPS Associated Protein involved in the apical positioning of rhoptries, and demonstrated that it plays a key role similar to that of TgARO in the final steps of rhoptry biogenesis, leading to apical translocation and firm positioning of these organelles to the parasite apex. Nevertheless, the comparative phenotypic analysis between these two mutants shows differences between the partners of the two proteins and their respective localizations. It has been shown that TgARO not only positions the rhoptries to the apical pole, but also maintains them in bundles. Our results show that TgCSCHAP mainly positions rhoptries at the apex but intervenes modestly in their clustering. Our findings suggest that TgCSCHAP is not a key player of the molecular machinery involved in clustering rhoptries with each other. Thus, TgARO and TgCSCHAP could act synergistically to attach rhoptries to each other and to position them in groups at the apex of the parasite, respectively. TgARO interaction with TgMyoF strongly suggests that the repositioning of the rhoptries is an actomyosin-based process. We have demonstrated that TgCSCHAP interacts with CORVET and HOPS tethering complexes and contains two putative binding domains to microtubules. This information raises the possibility of the existence of a new molecular machinery possibly depending on tubulin, involved in the positioning of rhoptries at the apex in coccidia. In this context, several studies have already highlighted a crosstalk between the dynactin complex and two subunits of the CORVET and HOPS tethering complexes (RILP and Vps18) during the vesicular transport and fusion stages [39,40]. It is conceivable that the TgCSCHAP protein, which contains a putative dynactin domain, assumes its function in the positioning of the rhoptries at the apex by ensuring the link between the CORVET/HOPS complexes, the rhoptries and the dynein/kinesin motors. In order to understand this key mechanism for parasite survival, the potential dynein and/or kinesin motors involved in the process are yet to be identified. Moreover, direct partners of TgCSCHAP need to be elucidated. Co-localization experiments have shown that TgCSCHAP exceeds the labeling surface covered by TgARO and is likely to be in the inner conoid below CAM1. It is

tempting to speculate that TgCSCHAP likely crosslink the rhoptries package to the two intraconoid microtubules and/or the microtubule filaments that are present at the inner part of the conoid. Finally, our results do not show an effect on the transport of secretory organelle proteins, as is the case in the Vps11 mutant [13], but show that the depletion of TgCSCHAP leads to the biogenesis of aberrant organelles in the apical region flanking the conoid. This could result either from abnormal microneme biogenesis or from the formation of chimeric compartments due to improper fusion events, and/or absence of docking. The exact nature of these structures will require further studies. We also established a specific effect on the positioning of rhoptries. Taken together, these observations suggest that TgCSCHAP is an additive component of CORVET and HOPS complexes and is likely to associate transiently with tethering complexes to accomplish particular functions important for the biogenesis and function of apical secretory organelles.

Acknowledgements

We thank Dominique Soldati-Favre, Vern Carruthers, Jean-François Dubremetz, Peter Bradley, Ke Hu, Gary Ward, David Sibley and David Roos for their kind gift of cell lines, plasmids or antibodies. We also thank the “Montpellier Ressources imagerie” platform and the electron microscopy facility of the University (MEA, “Microscopie Electronique et Analytique” for providing access to their microscopes. This work was made possible through core support from the Fondation pour la Recherche Médicale (Equipe FRMDEQ20130326508) and the Labex Parafrap (ANR-11-LABX-0024). MM was supported by an ERC Starting grant, (ERC-2012-StG 309255), and a Wellcome Senior Fellowship, 087582/Z/08/Z.

References

- [1] K. Hu, J. Johnson, L. Florens, M. Fraunholz, S. Suravajjala, C. DiLullo, J. Yates, D.S. Roos, J.M. Murray, Cytoskeletal components of an invasion machine—the apical complex of *Toxoplasma gondii*, *PLoS Pathog.* 2 (2006) e13.
- [2] K. Frenal, J.F. Dubremetz, M. Lebrun, D. Soldati-Favre, Gliding motility powers invasion and egress in Apicomplexa, *Nat. Rev. Microbiol.* 15 (2017) 645–660.
- [3] K. Hu, D.S. Roos, J.M. Murray, A novel polymer of tubulin forms the conoid of *Toxoplasma gondii*, *J. Cell. Biol.* 156 (2002) 1039–1050.
- [4] R. Mondragon, E. Frixione, Ca²⁺-dependence of conoid extrusion in *Toxoplasma gondii* tachyzoites, *J. Eukaryot. Microbiol.* 43 (1996) 120–127.
- [5] A.T. Heaslip, S.C. Ems-McClung, K. Hu, TgICMAP1 is a novel microtubule binding protein in *Toxoplasma gondii*, *PLoS One* 4 (2009) e7406.
- [6] J.C. Boothroyd, J.F. Dubremetz, Kiss and spit: the dual roles of *Toxoplasma* rhoptries, *Nat. Rev. Microbiol.* 6 (2008) 79–88.
- [7] J.P. Dubey, D.S. Lindsay, C.A. Speer, Structures of *Toxoplasma gondii* tachyzoites, bradyzoites, and sporozoites and biology and development of tissue cysts, *Clin. Microbiol. Rev.* 11 (1998) 267–299.
- [8] M.A. Hakimi, P. Olias, L.D. Sibley, *Toxoplasma* effectors targeting host signaling and transcription, *Clin. Microbiol. Rev.* 30 (2017) 615–645.
- [9] L.E. Kemp, M. Yamamoto, D. Soldati-Favre, Subversion of host cellular functions by the apicomplexan parasites, *FEMS Microbiol. Rev.* 37 (2013) 607–631.
- [10] B.P. Jena, Porosome: the secretory portal in cells, *Biochemistry* 48 (2009) 4009–4018.
- [11] S. Besteiro, J.F. Dubremetz, M. Lebrun, The moving junction of apicomplexan parasites: a key structure for invasion, *Cell. Microbiol.* 13 (2011) 797–805.
- [12] E. Jimenez-Ruiz, J. Morlon-Guyot, W. Daher, M. Meissner, Vacuolar protein sorting mechanisms in apicomplexan parasites, *Mol. Biochem. Parasitol.* 209 (2016) 18–25.
- [13] J. Morlon-Guyot, S. Pastore, L. Berry, M. Lebrun, W. Daher, *Toxoplasma gondii* Vps11, a subunit of HOPS and CORVET tethering complexes, is essential for the biogenesis of secretory organelles, *Cell. Microbiol.* 17 (2015) 1157–1178.
- [14] J.R. Beck, C. Fung, K.W. Straub, I. Coppens, A.A. Vashisht, J.A. Wohlschlegel, P.J. Bradley, A *Toxoplasma* palmitoyl acyl transferase and the palmitoylated armadillo repeat protein TgARO govern apical rhoptry tethering and reveal a critical role for the rhoptries in host cell invasion but not egress, *PLoS Pathog.* 9 (2013) e1003162.
- [15] C. Mueller, N. Klages, D. Jacot, J.M. Santos, A. Cabrera, T.W. Gilberger, J.F. Dubremetz, D. Soldati-Favre, The *Toxoplasma* protein ARO mediates the apical positioning of rhoptry organelles, a prerequisite for host cell invasion, *Cell Host Microbe* 13 (2013) 289–301.
- [16] C. Mueller, A. Samoo, P.M. Hammoudi, N. Klages, J.P. Kallio, I. Kursula, D. Soldati-Favre, Structural and functional dissection of *Toxoplasma gondii* armadillo repeats only protein, *J. Cell Sci.* 129 (2016) 1031–1045.
- [17] D. Jacot, W. Daher, D. Soldati-Favre, *Toxoplasma gondii* myosin F, an essential

- motor for centrosomes positioning and apicoplast inheritance, *EMBO J.* 32 (2013) 1702–1716.
- [18] M.H. Huynh, V.B. Carruthers, Tagging of endogenous genes in a *Toxoplasma gondii* strain lacking Ku80, *Eukaryot. Cell* 8 (2009) 530–539.
- [19] L. Sheiner, J.L. Demerly, N. Poulsen, W.L. Beatty, O. Lucas, M.S. Behnke, M.W. White, B. Striepen, A systematic screen to discover and analyze apicoplast proteins identifies a conserved and essential protein import factor, *PLoS Pathog.* 7 (2011) e1002392.
- [20] K. Kim, D. Soldati, J.C. Boothroyd, Gene replacement in *Toxoplasma gondii* with chloramphenicol acetyltransferase as selectable marker, *Science* 262 (1993) 911–914.
- [21] R.G. Donald, D.S. Roos, Stable molecular transformation of *Toxoplasma gondii*: a selectable dihydrofolate reductase-thymidylate synthase marker based on drug-resistance mutations in malaria, *Proc. Natl. Acad. Sci. U. S. A.* 90 (1993) 11703–11707.
- [22] A. Herm-Gotz, C. Agop-Nersesian, S. Munter, J.S. Grimley, T.J. Wandless, F. Frischknecht, M. Meissner, Rapid control of protein level in the apicomplexan *Toxoplasma gondii*, *Nat. Methods* 4 (2007) 1003–1005.
- [23] M. Meissner, S. Brecht, H. Bujard, D. Soldati, Modulation of myosin A expression by a newly established tetracycline repressor-based inducible system in *Toxoplasma gondii*, *Nucleic Acids Res.* 29 (2001) E115.
- [24] J. Morlon-Guyot, L. Berry, C.T. Chen, M.J. Gubbels, M. Lebrun, W. Daher, The *Toxoplasma gondii* calcium-dependent protein kinase 7 is involved in early steps of parasite division and is crucial for parasite survival, *Cell. Microbiol.* 16 (2014) 95–114.
- [25] A. Graindorge, K. Frenal, D. Jacot, J. Salamun, J.B. Marq, D. Soldati-Favre, The conoid associated motor MyoH is indispensable for *Toxoplasma gondii* entry and exit from host cells, *PLoS Pathog.* 12 (2016) e1005388.
- [26] K. Kremer, D. Kamin, E. Rittweger, J. Wilkes, H. Flammer, S. Mahler, J. Heng, C.J. Tonkin, G. Langsley, S.W. Hell, V.B. Carruthers, D.J. Ferguson, M. Markus, An overexpression screen of *Toxoplasma gondii* Rab-GTPases reveals distinct transport routes to the micronemes, *PLoS Pathog.* 9 (2013) e1003213.
- [27] J.Q. Tran, J.C. de Leon, C. Li, M.H. Huynh, W. Beatty, N.S. Morrisette, RNG1 is a late marker of the apical polar ring in *Toxoplasma gondii*, *Cytoskeleton (Hoboken)* 67 (2010) 586–598.
- [28] G. Couvreur, A. Sadak, B. Fortier, J.F. Dubremetz, Surface antigens of *Toxoplasma gondii*, *Parasitology* 97 (1988) 1–10.
- [29] A. Achbarou, O. Mercereau-Puijalon, J.M. Autheman, B. Fortier, D. Camus, J.F. Dubremetz, Characterization of microneme proteins of *Toxoplasma gondii*, *Mol. Biochem. Parasitol.* 47 (1991) 223–233.
- [30] A. Achbarou, O. Mercereau-Puijalon, A. Sadak, B. Fortier, M.A. Leriche, D. Camus, J.F. Dubremetz, Differential targeting of dense granule proteins in the parasitophorous vacuole of *Toxoplasma gondii*, *Parasitology* 103 (1991) 321–329.
- [31] M.H. Lamarque, M. Roques, M. Kong-Hap, M.L. Tonkin, G. Rugarabamu, J.B. Marq, D.M. Penarete-Vargas, M.J. Boulanger, D. Soldati-Favre, M. Lebrun, Plasticity and redundancy among AMA-RON pairs ensure host cell entry of *Toxoplasma* parasites, *Nat. Commun.* 5 (2014) 4098.
- [32] E.T. Larson, F. Parussini, M.H. Huynh, J.D. Giebel, A.M. Kelley, L. Zhang, M. Bogyo, E.A. Merritt, V.B. Carruthers, *Toxoplasma gondii* cathepsin L is the primary target of the invasion-inhibitory compound morpholinurea-leucyl-homophenyl-vinyl sulfone phenyl, *J. Biol. Chem.* 284 (2009) 26839–26850.
- [33] K. Frenal, V. Polonais, J.B. Marq, R. Stratmann, J. Limenitakis, D. Soldati-Favre, Functional dissection of the apicomplexan glideosome molecular architecture, *Cell Host Microbe* 8 (2010) 343–357.
- [34] W. Daher, F. Plattner, M.F. Carlier, D. Soldati-Favre, Concerted action of two formins in gliding motility and host cell invasion by *Toxoplasma gondii*, *PLoS Pathog.* 6 (2010) e1001132.
- [35] M. Lebrun, A. Michelin, H. El Hajj, J. Poncet, P.J. Bradley, H. Vial, J.F. Dubremetz, The rhoptyr neck protein RON4 re-localizes at the moving junction during *Toxoplasma gondii* invasion, *Cell. Microbiol.* 7 (2005) 1823–1833.
- [36] J. Morlon-Guyot, H. El Hajj, K. Martin, A. Fois, A. Carrillo, L. Berry, R. Burchmore, M. Meissner, M. Lebrun, W. Daher, A proteomic analysis unravels novel CORVET and HOPS proteins involved in *Toxoplasma gondii* secretory organelles biogenesis, *Cell. Microbiol.* (2018) e12870.
- [37] Y. Chen, Z.H. Sheng, Kinesin-1-synthaphilin coupling mediates activity-dependent regulation of axonal mitochondrial transport, *J. Cell. Biol.* 202 (2013) 351–364.
- [38] J.J. Liu, Regulation of dynein-dynactin-driven vesicular transport, *Traffic* 18 (2017) 336–347.
- [39] R. van der Kant, A. Fish, L. Janssen, H. Janssen, S. Krom, N. Ho, T. Brummelkamp, J. Carette, N. Rocha, J. Neeffes, Late endosomal transport and tethering are coupled processes controlled by RILP and the cholesterol sensor ORP1L, *J. Cell Sci.* 126 (2013) 3462–3474.
- [40] X. Xiang, R. Qiu, X. Yao, H.N. Jr, M.A. Arst, J. Penalva, Zhang, Cytoplasmic dynein and early endosome transport, *Cell. Mol. Life Sci.* 72 (2015) 3267–3280.